Formation and motion of a transpolar arc in response to dayside and nightside reconnection

S. E. Milan, B. Hubert,[1] and A. Grocott

Department of Physics and Astronomy, University of Leicester, Leicester, UK

[1]   We trace the formation and subsequent motion of a transpolar arc in response to dayside and nightside reconnection. Both high- and low-latitude dayside reconnection are observed, as well as periods of substorm and nonsubstorm nightside reconnection, during the 7-hour interval of interest on 19 January 2002. We speculate that the arc is formed by a burst of nonsubstorm nightside reconnection and that its subsequent motion is controlled predominantly by the rate of dayside high-latitude reconnection, siphoning open flux from the dusk sector polar cap to the dawn sector. The observations allow us to quantify the rates of reconnection: on the nightside, 35 and 100 kV during nonsubstorm- and substorm-related bursts, respectively; on the dayside, 30 and 100 kV for high- and low-latitude reconnection. The latter values give effective merging line lengths of 1 and 5.5 R_E for northward and southward interplanetary magnetic field, respectively. We suggest that transpolar arc motion will be controlled not only by the B_y component of the IMF but also by the relative magnitude of the B_z component, when $|B_y| > B_z$ motion will be dawnward for $B_y < 0$ nT and duskward for $B_y > 0$ nT; however, when $B_z > |B_y|$, we expect that the arc will move toward the noon-midnight meridian of the polar cap.

Citation: Milan, S. E., B. Hubert, and A. Grocott (2005), Formation and motion of a transpolar arc in response to dayside and nightside reconnection, *J. Geophys. Res.*, *110*, A01212, doi:10.1029/2004JA010835.

1.   Introduction

[2]   Recent studies have shown that observations of the polar ionosphere can be used to monitor changes in the amount of open magnetic flux in the magnetosphere, from which the rates of low-latitude dayside reconnection and nightside magnetotail reconnection can be deduced (e.g., most recently, *Taylor et al.* [1996], *Mishin et al.* [1997], *Milan et al.* [2003, 2004], and *Milan* [2004b]). Increases in the area of the polar cap are symptomatic of the creation of new open flux by reconnection at the low-latitude magnetopause (that is, by reconnection of interplanetary magnetic field lines with closed terrestrial field lines), whereas a decrease in polar cap area indicates the onset of reconnection in the magnetotail. However, this does not allow a quantification of the reconnection rate at a high-latitude, or lobe, reconnection site, which is expected to occur when the interplanetary magnetic field (IMF) has a significant northward component [e.g., *Russell*, 1972; *Cowley*, 1981; *Reiff and Burch*, 1985; *Cowley and Lockwood*, 1992]. This is because lobe reconnection does not change the amount of open flux in the magnetosphere but rather stirs the open flux that is already present. As a

consequence the rate at which lobe reconnection occurs and the factors which control this are presently not well known, though some estimates have been made from, for instance, ionospheric flow data [*Huang et al.*, 2000; *Chisham et al.*, 2004].

[3]   Another phenomenon associated with periods of northward IMF is the appearance of auroral arcs within the polar cap, sometimes known as transpolar arcs or, when they stretch almost entirely across the polar cap, as theta aurora (*Frank et al.* [1982, 1986]; see also review by *Zhu et al.* [1997]). In the main these arcs are thought to be the optical manifestation of particle precipitation on closed field lines. This indicates that under northward IMF conditions the polar cap can become bisected by a tongue of closed flux emanating from the nightside auroral oval, with ramifications for magnetotail structure that have been discussed by, e.g., *Frank et al.* [1986], *Huang et al.* [1987], and *Zhu et al.* [1997]. Under these circumstances the polar cap can be thought of as containing two compartments of open flux partitioned by the transpolar arc, and these compartments map to a bifurcated lobe. The motion of transpolar arcs across the polar cap from dawn to dusk and vice versa is controlled to a large extent by the B_y component of the IMF [e.g., *Frank et al.*, 1986; *Rairden and Mende*, 1989; *Valladares et al.*, 1994; *Kullen et al.*, 2002], suggesting that these dynamics are associated with magnetic reconnection.

[4]   In this paper we demonstrate that indeed the motion of such arcs is probably controlled by the rate of lobe

---

[1]Also at Laboratory of Planetary and Atmospheric Physics, University of Liege, Liege, Belgium.
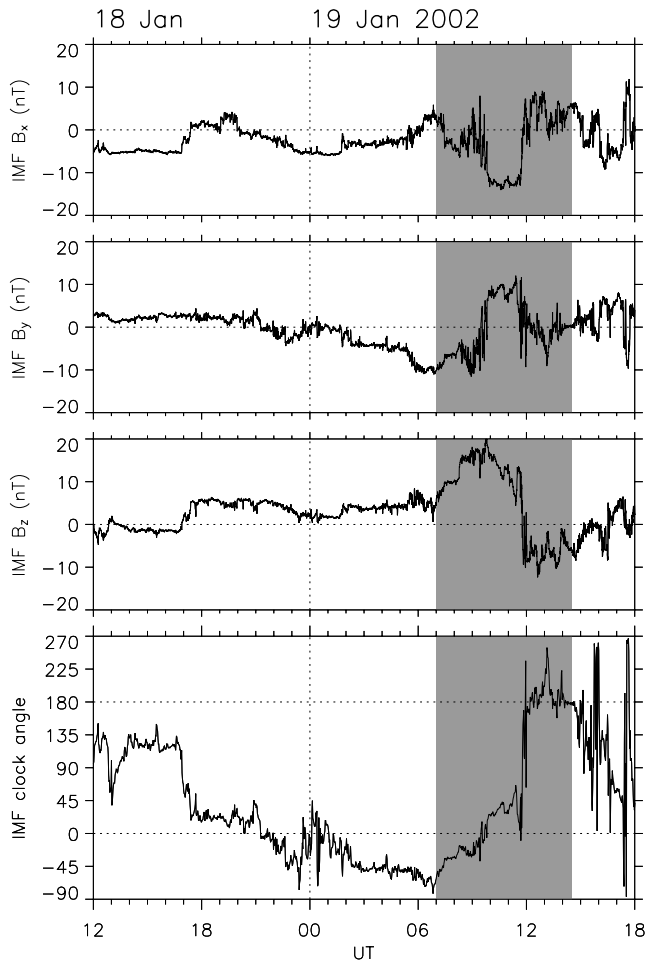
Figure 1. GSM B_x, B_y, and B_z interplanetary magnetic field components, along with the corresponding clock angle, measured during a 30-hour interval on 18 and 19 January 2002 by the ACE spacecraft. Period pertaining to the ionospheric observations is highlighted in grey.

reconnection transferring open flux from one polar cap compartment to the other. Thus the motion of the transpolar arc, or more importantly, the inflation of one polar cap compartment, and the corresponding deflation of the other, can be used to quantify the rate of lobe reconnection. We compare observations of the polar aurora from the Imager for Magnetopause-to-Aurora Global Exploration (IMAGE) FUV/Wide-band Imaging Camera (WIC) instrument [*Mende et al.*, 2000a, 2000b] with simultaneous measurements of the ionospheric convection flow by the Super Dual Auroral Radar Network (SuperDARN) [*Greenwald et al.*, 1995] to quantify reconnection rates at the low- and high-latitude magnetopause and in the magnetotail.

2. Observations

[5] Figure 1 shows the upstream IMF conditions in GSM coordinates as measured by the magnetometer instrument onboard the ACE spacecraft [*Smith et al.*, 1998], between 1200 UT on 18 January and 1800 UT on 19 January 2002. These data have been time lagged by 75 min to account for the propagation delay from ACE, located near the L1 Lagrangian point, to the magnetopause and the subsequent

propagation of information to the ionosphere. This lag was calculated given the location of ACE at $X \approx 240$ R_E and a solar wind speed of $\sim$350 km s^{-1}, as measured by the Solar Wind Electron, Proton, and Alpha Monitor instrument [*McComas et al.*, 1998]. Our interval of interest, 0700–1430 UT on 19 January, highlighted in grey in Figure 1, occurred toward the end of an extended period of northward IMF. The B_y component changed from negative to positive at 0930 UT, at which time B_z reached a maximum of 15 nT. Thereafter B_z decreased and turned negative at 1145 UT, and B_y became near zero. These variations are reflected in the IMF clock angle, which progressed relatively smoothly from $-70°$ to $70°$ between 0700 and 1145 UT and thereafter settled near $180°$.
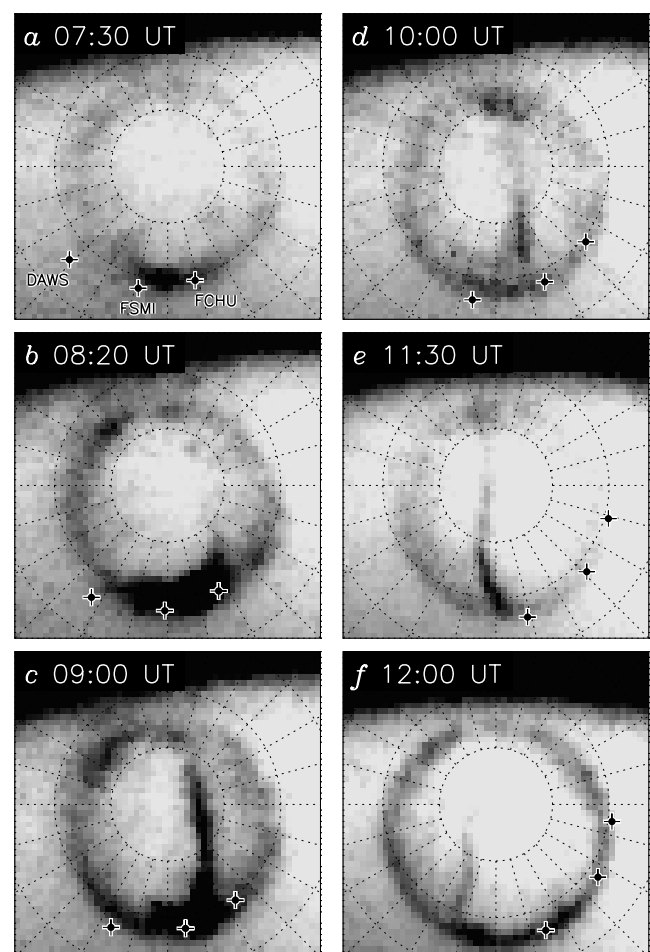

Figure 2. (a–f) Six snapshots of the Northern Hemisphere auroral configuration during the period of interest by the Imager for Magnetopause-to-Aurora Global Exploration (IMAGE) FUV/Wide-band Imaging Camera (WIC) instrument, presented in a magnetic latitude and magnetic local time frame, with noon toward the top of each panel. Concentric circles mark magnetic latitudes of 60°, 70°, and 80°. Darker shading indicates brighter aurora. Locations of three Canadian Auroral Network for the OPEN Program Unified Study (CANOPUS) stations, Dawson (DAWS), Fort Smith (FSMI), and Fort Churchill (FCHU), are also indicated.
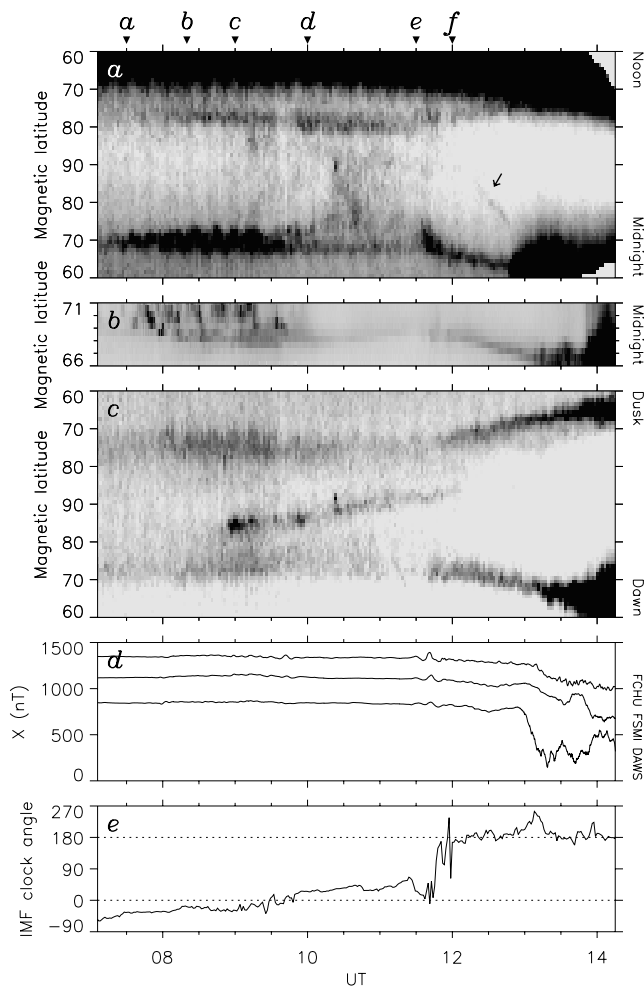
Figure 3. (a) A keogram of the IMAGE FUV/WIC observations along the noon-midnight meridian. Times of the auroral snapshots of Figure 2 are indicated at the top by arrows. (b) A 557.7-nm keogram of the FSMI meridian-scanning photometer, corresponding approximately to the nightside portion of Figure 3a. (c) IMAGE FUV/WIC keogram from the dawn-dusk meridian. (d) X-component magnetograms from the DAWS, FSMI, and FCHU stations. Variations shown are relative, an arbitrary baseline having been removed from each trace. (e) IMF clock angle.

[6] Figures 2a–2f show a sequence of auroral images taken by the FUV/WIC instrument onboard the IMAGE spacecraft. Dayglow is evident at the top of each image; otherwise, darker shades indicate brighter aurora. The sequence of images shows a dim, somewhat contracted oval, with some evidence of a nightside brightening (Figure 2a); further brightening on the nightside and the formation of a transpolar arc in the postmidnight sector (Figures 2b and 2c); a progression of the transpolar arc from dawn toward dusk (Figures 2d and 2e); and a confinement of the arc in the premidnight sector (Figure 2f), the arc appearing to shrink away from the dayside as the auroral oval as a whole expands to lower latitudes. The locations of three stations of the Canadian Auroral Network for the OPEN Program Unified Study (CANOPUS) network (described by *Samson et al.* [1992]), Dawson (DAWS), Fort Smith (FSMI), and

Fort Churchill (FCHU), are indicated in each panel. We will employ magnetograms from all three stations to identify substorm onset; in addition, FSMI houses a meridian-scanning photometer, which we use to supplement the spaceborne imager.

[7] To gain a better understanding of the motion of the transpolar arc and the auroral oval, Figure 3 shows keograms of the FUC/WIC auroral observations along the noon-midnight (Figure 3a) and dawn-dusk (Figure 3c) meridians. Also included in Figure 3 are 557.7-nm auroral observations from the FSMI meridian-scanning photometer (Figure 3b), roughly coincident with the midnight meridian of Figure 3a; X-component magnetograms from DAWS, FSMI, and FCHU (Figure 3d); and the IMF clock angle (Figure 3e). The times of the auroral snapshots in Figure 2 are indicated at the top of the diagram by arrows. Dayglow in the sunlit hemisphere is apparent in Figure 3a, but clear also is the auroral oval on both the dayside and the nightside. In Figure 3c the auroral oval is visible in both dawn and dusk sectors, and near the center of the polar cap the transpolar arc is also apparent. From these observations it is clear that the auroral oval remained at an approximately constant latitude from 0700 until 1140 UT, during the period that IMF $B_z > 0$ nT, whereafter it smoothly proceeded to lower latitude, after the southward turning of the IMF to $B_z < 0$ nT. A brightening of the nightside oval is seen from ~0730 until ~0930 UT, and a clear substorm breakup is seen at 1245 UT. For most of the interval the magnetograms remain very quiet, though with the clear signature of sub-storm breakup shortly before 1300 UT, corresponding to the onset determined from the auroral observations; no magnetogram signatures are observed during the initial auroral brightening period, 0730–0930 UT. We note at this point an interesting feature in Figure 3a: a faint auroral feature, marked by an arrow, that starts near the dayside auroral oval at the time of the southward turning (1140 UT), crosses the polar cap, and disappears into the nightside substorm breakup aurora at 1300 UT. This feature marks the sunward end of the transpolar arc, as will be discussed in more detail in section 3.4.

[8] The transpolar arc first formed near 0820 UT (Figure 2b) and remained visible until shortly before 1300 UT. However, it was not apparent in the keogram of Figure 3c until 0850 UT and disappeared from the dawn-dusk meridian near 1200 UT, shortly after the southward turning of the IMF. During this interval a steady progression of the arc from dawn to dusk can clearly be seen in Figure 3c, irrespective of whether IMF $B_y < 0$ or $B_y > 0$, though the duskward motion is perhaps most rapid after the IMF turned from $B_y < 0$ to $B_y > 0$ at 0945 UT. In other words, during this interval the motion of the arc does not appear to be directly linked to the dawn-dusk orientation of the IMF, in contrast to reports by previous authors [e.g., *Valladares et al.*, 1994; *Kullen et al.*, 2002].

[9] The open flux contained within the magnetosphere was determined from the size of the dim polar cap in the auroral measurements, using the techniques described by *Milan et al.* [2003, 2004], and the variation in this as a function of time is shown in Figure 4. The total open flux F_{PC} is shown as the thick solid curve in Figure 4a. We also determined the partitioning of this flux by the transpolar arc into dawn- and dusk-sector polar caps, and these are shown
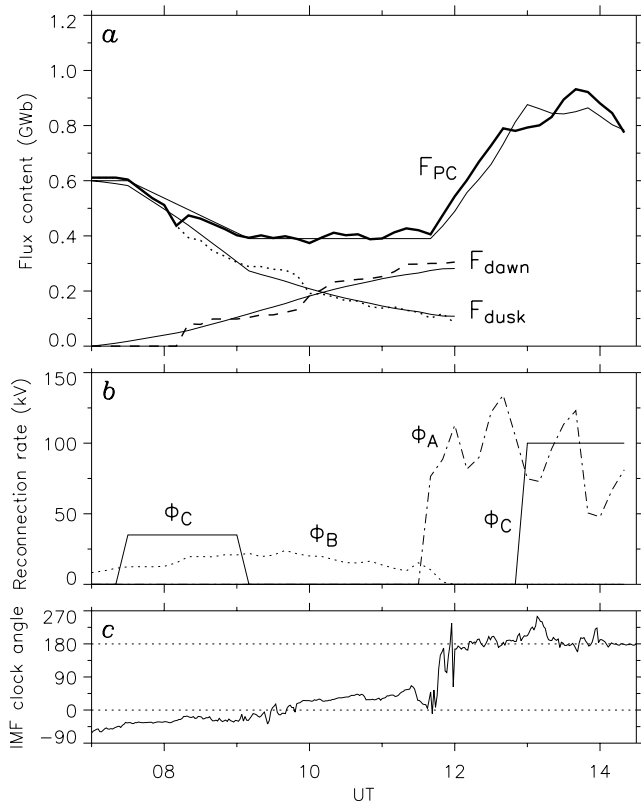
Figure 4. (a) Total polar cap flux, and the flux contained dawnward and duskward of the transpolar arc, determined from the auroral observations, indicated by thick solid, dashed, and dotted curves, respectively. Thin solid curves represent fits to these data, found using the (b) reconnection rates shown (see text for more details). Figure 4b shows estimated nightside reconnection rate, Φ_C, and low- and high-latitude dayside reconnection rates Φ_A and Φ_B, calculated from equations (2) and (5), respectively, for effective X-line lengths L_A and L_B of 5.5 and 0.5 R_E. (c) IMF clock angle.

by the quantities F_{dawn} and F_{dusk}, represented by dashed and dotted curves, respectively. We will discuss these findings in more detail in sections 3.1 and 3.3.

[10] Finally, we turn to the ionospheric convection measurements made by the SuperDARN radars, presented in Figure 5, superimposed on the IMAGE auroral observations previously shown in Figure 2 (though somewhat dimmed to aid clarity). These are produced by compiling 10-min averages of line-of-sight Doppler velocity observations from eight Northern Hemisphere radars, which are then used to constrain the solution of an order 8 spherical harmonic expansion of the potential pattern, using the technique of *Ruohoniemi and Baker* [1998]. Where data are sparse, an IMF-driven empirical convection model is employed to further constrain the potential pattern, though in the present case the data coverage was generally excellent, and the empirical model contributed only little to the final solutions. In Figure 5, contours show the resulting potential pattern, solid and dashed contours for negative and positive potentials, respectively, with a contour spacing of 6 kV. The vectors indicate the locations of radar observa-

tions that contributed to the potential solution; the length of these is related to the flow speed.

[11] The first potential pattern, from 0730 UT, Figure 5a, shows convection typical of northward IMF conditions. This includes sunward flow near noon with two "reverse convection" lobe cells, with centers near 80°, 1400 magnetic local time (MLT), and 85°, 0900 MLT, indicating the occurrence of high-latitude reconnection [e.g., *Russell*, 1972; *Cowley*, 1981; *Reiff and Burch*, 1985; *Cowley and Lockwood*, 1992; *Huang et al.*, 2000; *Milan et al.*, 2000; *Chisham et al.*, 2004]. These cells appear to be contained entirely within the polar cap, that is, are located poleward of the dayside auroral luminosity, as expected for this reconnection scenario. The two lobe cells are not exactly symmetrical about the noon-midnight meridian but are shifted toward the prenoon sector, as a consequence of the IMF $B_y < 0$ nT conditions that prevailed at this time. On the nightside, coincident with the auroral brightening first observed shortly before 0730 UT, relatively strong westward flows are seen in the midnight and premidnight sectors. These nightside flows are highly reminiscent of
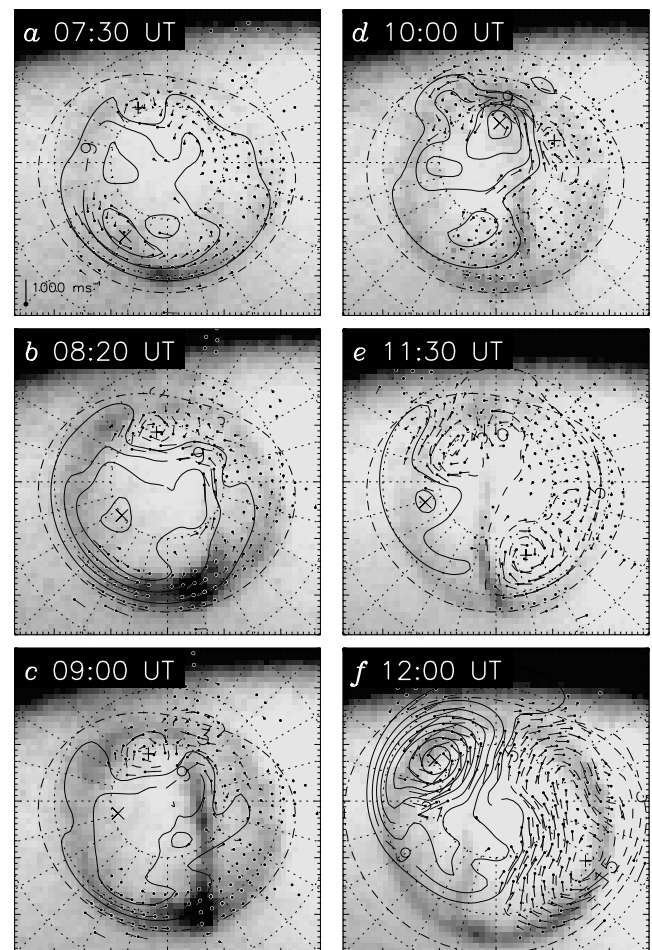

Figure 5. (a–f) Six auroral snapshots of Figure 2, with SuperDARN estimates of the simultaneous ionospheric convection overlaid. Vectors indicate the location of convection measurements. Fitted potential contours are separated by 6 kV.

those reported by *Senior et al.* [2002] and *Grocott et al.* [2003, 2004] which are observed during nonsubstorm episodes of magnetotail reconnection occurring when the IMF is directed northward. They found that such flows tend to be directed east-west for $B_y < 0$ nT and west-east for $B_y > 0$ nT, consistent with the present observations.

[12] A very similar flow pattern is observed in Figure 5b, at 0820 UT, though in this case the dayside flows are perhaps somewhat enhanced. At this time the initial development of the transpolar arc is apparent; the nightside westward flows are contained to the west of this nascent arc. In the next auroral snapshot, at 0900 UT, Figure 5c, the transpolar arc is well developed. The flow measurements have not changed substantially at this time, though the nightside flows are somewhat diminished. Again, these nightside flows are located to the west of the transpolar arc. The postnoon lobe convection cell is contained entirely within the dusk-sector polar cap. Interestingly, the prenoon lobe cell convection appears to begin in the dusk-sector polar cap and to be directed sunward and then westward, such that it skirts the sunward end of the transpolar arc and enters the dawn-sector polar cap. At 1000 UT, Figure 5d, the nightside flows have diminished almost entirely, though the dayside flows, especially from dusk-sector to dawn-sector polar caps, are enhanced. The sunward flow region associated with the reverse convection is now located postnoon, consistent with expectations [e.g., *Cowley and Lockwood*, 1992], as B_y has become positive at this time.

[13] At 1130 UT, Figure 5e, the lobe convection cells are still present, though the flow speeds have decreased. There is now some enhanced convection on the nightside, apparently confined to the nightside dawn-sector polar cap, though there are no flow measurements premidnight to confirm that this confinement is real. Finally, we turn to Figure 5f, 1200 UT, which shows the development of a strong twin-cell convection pattern, as expected following the southward turning of the IMF after 1145 UT. Unfortunately, no flow measurements are available in the premidnight sector, into which the transpolar arc is being pushed. In section 3 we discuss the formation, motion, and subsequent decay of the transpolar arc in terms of the convection flows measured by SuperDARN and a theoretical understanding of the coupling between the solar wind and the magnetosphere.

3. Discussion

[14] Our observations show the development and subsequent motion of a transpolar arc during an interval of northward IMF. Before discussion of the formation and subsequent motion of the arc itself, we examine the solar wind−magnetosphere coupling expected to occur during the event, which previous studies lead us to believe that we now understand relatively well [e.g., *Milan et al.*, 2003, 2004; *Milan*, 2004a, 2004b].

3.1. Polar Cap Dynamics

[15] The start of the period of interest, from 0700 until 1145 UT, is characterized by northward IMF; thereafter, the IMF turned southward. During the first interval we expect high-latitude reconnection to occur between the IMF and magnetotail lobe field lines; during the second interval, low-latitude or subsolar reconnection between closed terrestrial field lines and the IMF is expected. The latter process creates new open flux, causing the polar cap to expand and the auroral oval to move to lower latitudes; the former process does not, and the polar cap remains of constant size unless nightside reconnection occurs. We now show that these expectations are consistent with the observations during the present interval.

[16] The transpolar arc forms at the eastward edge of a nightside auroral brightening associated with westward plasma convection, argued by *Grocott et al.* [2003, 2004] to be the signature of magnetotail closure of open flux during northward IMF, nonsubstorm intervals; the CANOPUS magnetograms confirm that substorm signatures are absent at this time. It is now clear that such reconnection bursts are an important component of the flux transfer mechanism within the magnetosphere, and we coin the phrase "tail reconnection during IMF-northward, nonsubstorm intervals" (TRINNIs) to describe them. From the auroral observations we estimate that prior to the onset of the nightside brightening associated with the TRINNI, the polar cap contained $F_{PC} \approx 0.6$ GWb of open flux (Figure 4). During the nightside brightening, from 0730 until 0900 UT, this flux decreased until F_{PC} reached 0.4 GWb, representing a flux closure rate of ∼35 kV. After ∼0900 UT, tail reconnection ceased and the total flux content of the magnetosphere remained constant until the southward turning of the IMF at ∼1145 UT. At this point, F_{PC} began to increase rapidly as subsolar magnetopause reconnection commenced, driving the development of a twin-cell convection pattern characteristic of southward IMF. For instance, in Figure 5f, flow can clearly be seen crossing the dayside auroral oval from low latitudes to high latitudes as the auroral oval progresses to lower latitudes (see Figure 3), indicating the creation of new open flux and the associated expansion of the polar cap. At 1245 UT, substorm expansion phase onset was observed in both the auroral observations and magnetograms (Figure 3). The growth of the polar cap was slowed and then reversed to contraction (Figure 4), as substorm tail reconnection commenced and then dominated over the dayside reconnection rate.

[17] As described by *Milan* [2004b, and references therein], it is straightforward to deduce the rates of dayside and nightside reconnection from observations of the polar cap area and upstream IMF conditions. Changes in polar cap flux content are controlled by Faraday's law, cast in the following form [e.g., *Siscoe and Huang*, 1985]:

$$\frac{dF_{PC}}{dt} = \frac{d}{dt} \int_{PC} \mathbf{B} \cdot d\mathbf{s} = \Phi_A - \Phi_C, \tag{1}$$

where Φ_A and Φ_C are the rates of low-latitude dayside reconnection and magnetotail reconnection, respectively. $\mathbf{B}$ is the ionospheric magnetic field strength, the radial component of which, integrated over the polar cap, gives the open flux content of the magnetosphere. Dayside and nightside reconnection rates can be determined by fitting to the observed variation in F_{PC}. The rate of low-latitude dayside reconnection Φ_A can be predicted from the half wave rectified Y component of the upstream solar wind motional electric field, $V_x B_S$, integrated along an effective
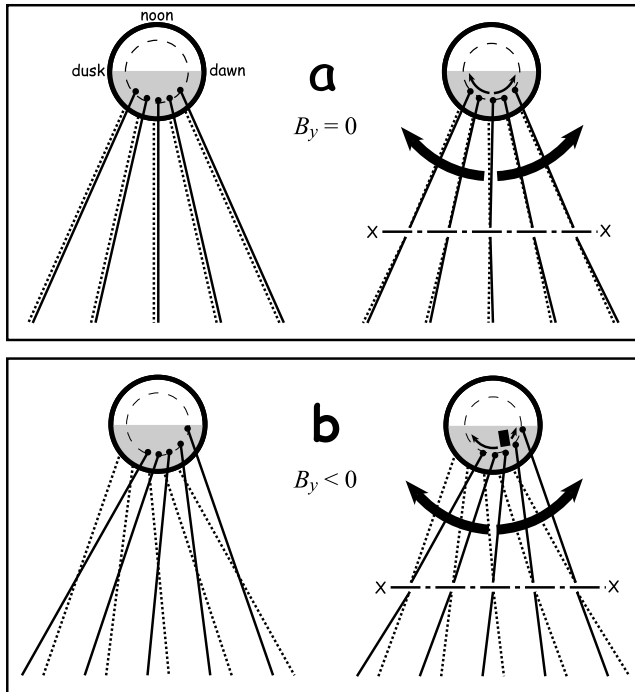
Figure 6. Representations of the magnetic field topologies in the magnetotail before and after reconnection, for (a) IMF $B_y = 0$ and (b) IMF $B_y < 0$. Earth is shown from over the northern magnetic pole, with noon located toward the top of the page. Polar cap is indicated by the dashed circle, and nightside field lines are indicated as solid (dotted) lines for the Northern (Southern) Hemisphere. Convection return flows in the equatorial plane of the tail and in the ionosphere are shown by arrows. In Figure 6b, opposing forces in the Northern and Southern Hemispheres result in the formation of a transpolar arc (black rectangle).

scale length L_A which takes a value between 5 and 8 R_E [*Milan*, 2004a, 2004b]:

$$\Phi_A = V_x B_S L_A, \qquad (2)$$

where B_S is the southward component of the IMF, i.e.,

$$B_S = \begin{cases} 0 & B_z > 0 \\ -B_z & B_z < 0 \end{cases}. \qquad (3)$$

Φ_A, so predicted using a value of $L_A = 5.5$ R_E, is shown in Figure 4b. The cross-wind scale of the magnetopause is of the order of 25 R_E, suggesting that the reconnection efficiency is close to 20–25% [e.g., *Holzer and Slavin*, 1979; *Reiff et al.*, 1981; *Milan*, 2004a, 2004b]. We also assume that the nightside auroral brightening (0730 until 0900 UT) has associated with it a nightside reconnection rate of $\Phi_C = 35$ kV, as discussed above. Integration of Φ_A and Φ_C, using an initial value of F_{PC} of 0.6 GWb, fits well the observations until 1245 UT, when the polar cap ceases to expand as expected. The discrepancy between predicted and measured F_{PC} indicates that the tail reconnection rate associated with the substorm onset is of

the order of $\Phi_C = 100$ kV. Using this value, the thin overlaid curve in Figure 4a is found.

[18] We also note as a point of interest in passing that the TRINNI, although it has an average merging rate of 35 kV, is clearly pulsed quasiperiodically, with a repetition period of ∼20 min, as suggested by the pulsed nature of the FSMI meridian-scanning photometer observations (Figure 3b), and modulations of the associated convection velocity (for brevity not shown in the present study, but described also by *Senior et al.* [2002] and *Grocott et al.* [2003, 2004]). We leave this as a topic for further investigation. Further study is also needed to understand why there is an absence of magnetogram signatures during this reconnection event, despite periodically varying convection and auroral signatures at this time.

3.2. Formation of the Transpolar Arc

[19] The transpolar arc forms during the TRINNI event described in section 3.1. Here we speculate that the occurrence of the TRINNI and the formation of the transpolar arc are linked.

[20] *Grocott et al.* [2003, 2004] surmised that the direction of the flow leaving the polar cap (dawnward or duskward) during TRINNIs is modulated by the prevalent IMF B_y orientation in the recent past. This control is exerted due to the dawn-dusk forces exerted on newly opened field lines by the B_y orientation and the dawn-dusk component of the magnetic field that this introduces into the tail lobes as open field lines are stretched antisunward by the flow of the solar wind. Subsequent reconnection of these field lines in the tail creates new closed field lines which are not contained in meridian planes but which straddle the noon-midnight meridian plane of the tail, connecting the dawn and dusk sectors in opposite hemispheres. Figure 6 shows schematically tail field lines, before and after tail reconnection, for the cases of no imposed B_y in the tail (Figure 6a) and $B_y < 0$ (Figure 6b), the situation appropriate for the start of the interval of interest. Figure 6 shows the Earth looking down onto the north magnetic pole, with the Sun to the top of the page. A dashed circle shows the extent of the polar cap. Emanating from the nightside of the polar cap, five Northern Hemisphere lobe field lines (pointing toward the Earth) and five Southern Hemisphere lobe field lines (pointing away from the Earth) are shown by solid and dotted lines, respectively. In Figure 6a, when a tail X-line forms, the resulting closed field lines are contained in meridian planes, and as they contract and convect around the Earth toward the dayside, they generate dawnward and duskward return flow in the nightside ionosphere symmetrically about the noon-midnight meridian. In Figure 6b the addition of the B_y component to the tail skews the northern and southern lobe field lines with respect to each other. Now when reconnection takes place, the resulting closed field lines are no longer contained in meridian planes.

[21] This interesting topology results in strong westward flow in the midnight sector of the Northern Hemisphere ionosphere. The southern hemispheric ends of these field lines map to the dusk sector ionosphere and need only convect slowly in the return flow. Correspondingly, in the dawn sector of the Northern Hemisphere, slow or stagnant eastward return flow is expected as the southern hemispheric ends of these field lines attempt to catch up with vigorous
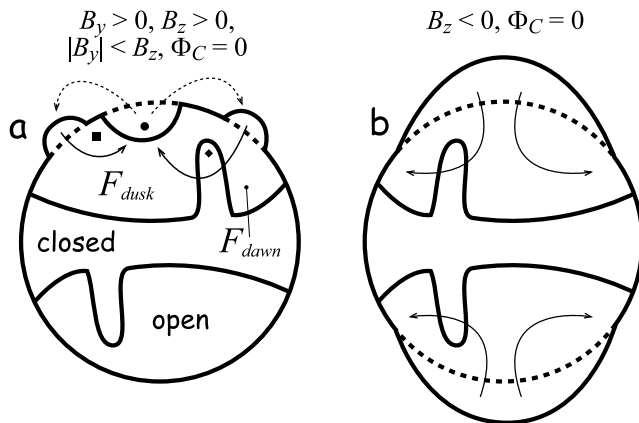
Figure 7. (a and b) Cross sections of the magnetotail, looking toward the Earth, with north toward the top. Open lobes are seen to the north and the south, sandwiched between which is the closed plasma sheet, including tongues of closed flux which map to the transpolar arc in the Northern Hemisphere and, we speculate, in the Southern Hemisphere.

eastward flow in the midnight sector. However, the field line that maps to the noon-midnight meridian in the equatorial plane faces competition between the Northern and Southern Hemispheres, as both ends of this field line cannot simply convect sunward in the return flow region as is the case in more simple field geometries.

[22] We speculate that this field topology, and the plasma and flux motions which result, may contribute to the formation of the transpolar arc, specifically the extrusion of closed plasma sheet field lines out of the equatorial plane of the magnetotail to bisect the lobes, as return flow is stymied by opposing tension forces between the opposite hemispheres. This would place the formation of the arc in the dawn (dusk) sectors at the eastern (western) end of a strong westward (eastward) convection jet for $B_y < 0$ ($B_y > 0$), consistent with the present observations. We expect these relationships to be reversed in the Southern Hemisphere.

[23] Figure 7a presents a schematic diagram of the envisaged configuration that the magnetotail takes following the onset of the TRINNI (the flows indicated will be described in section 3.3). The magnetotail is shown in cross section, looking toward the Earth. The northern and southern (open) lobes are separated by the (closed) plasma sheet, which is extended to the north and south in tongues of closed flux that map to the transpolar arc in the Northern Hemisphere and presumably a counterpart arc in the Southern Hemisphere, a configuration suggested by, e.g., *Frank et al.* [1986], *Huang et al.* [1987], and *Zhu et al.* [1997]. To the north of the equatorial plane, magnetic field lines point into the picture (toward the Earth), whereas below they point out of the page. Although at present we cannot be certain about the mapping of the transpolar arc field lines between the northern and southern lobes, for the reasons outlined above we show the initial configuration with the Northern Hemisphere arc displaced toward dawn and the Southern Hemisphere arc displaced toward dusk, though threaded by common flux. The exact nature of the inter-

hemispheric antisymmetry/symmetry of the TRINNI flows, and their relationship to transpolar arc formation, is as yet unclear due to a dearth of observations to date, and we leave this as an avenue for further investigation.

3.3. Motion of the Transpolar Arc

[24] Our observations suggest that in the presence of a transpolar arc the polar cap is partitioned into two regions dawnward and duskward of the arc, and high-latitude reconnection can siphon open flux from one region to the other, causing the arc to move. In this section we investigate this idea in more detail. Fortuitously, this also allows us to quantify the high-latitude reconnection rate, a measurement that is normally difficult to make, as estimates of the overall size of the polar cap do not reveal the level of coupling.
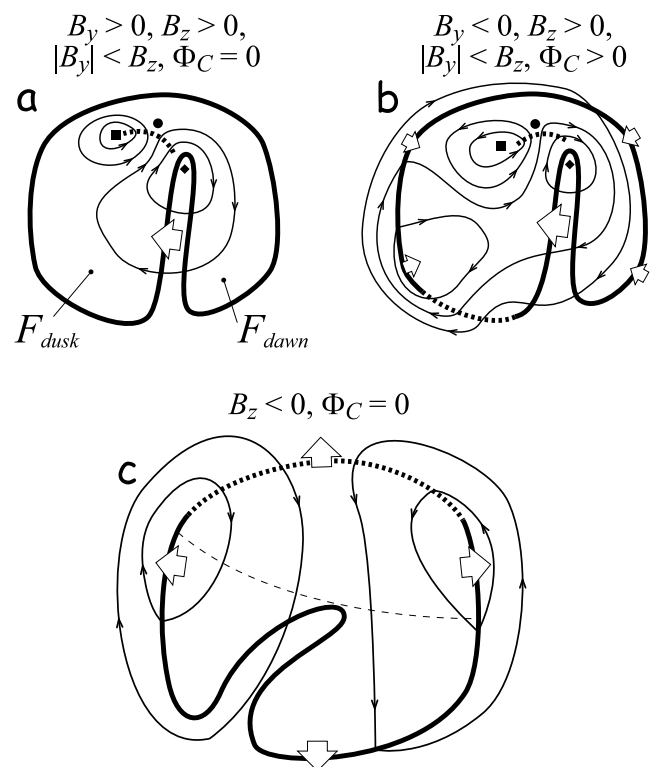

Figure 8. Schematic diagrams indicating the expected dynamics of the polar cap boundary, ionospheric convection flow, and transpolar arc, in response to (a) high-latitude dayside reconnection, (b) high-latitude dayside reconnection and nightside nonsubstorm reconnection, and (c) low-latitude dayside reconnection. Thick solid curves indicate the adiaroic open/closed field line boundary, and the thick dotted curves represent merging gaps. Thin arrowed curves show convection streamlines. Large arrows show motions of the open-closed field line boundary. In Figures 8a and 8b the square and diamond indicate the focii of the dusk and dawn reverse convection cells, respectively; the circle indicates the point at which flow is diverted dawnward or duskward after crossing the high-latitude merging gap, effectively separating the dawn and dusk cells. In Figure 8c the thin dashed curve shows the boundary between new and preexisting open flux. Figure 8a corresponds to Figure 7a, and Figure 8c corresponds to Figure 7b.
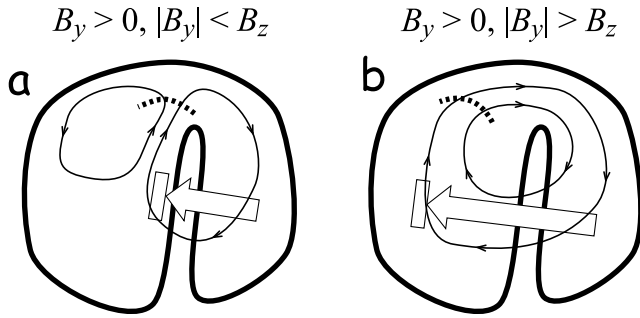
$$B_y > 0, |B_y| < B_z \qquad\qquad B_y > 0, |B_y| > B_z$$

Figure 9. Expected ionospheric convection patterns for IMF $B_z > 0$, for the cases (a) $|B_y| < B_z$ and (b) $|B_y| > B_z$; the patterns shown are appropriate for $B_y > 0$; for $B_y < 0$ the patterns would be a mirror image about the noon-midnight meridian. Large arrows show the direction and maximum extent of arc motion in response to the convection flow. In Figure 9a, if the transpolar arc was located in the dusk sector, motion would be dawnward toward the noon-midnight meridian. In Figure 9b, motion is duskward, irrespective of the location of the arc.

[25] Figure 8a shows schematically the polar cap, surrounded by the open-closed field line boundary ((OCB) heavy solid curve), with noon at the top of the figure. A tongue of closed flux, the transpolar arc, is seen to protrude into the polar cap, dividing it into a dawn and dusk region, corresponding to the magnetotail structure illustrated in Figure 7a. The dotted thick curve shows the ionospheric footprint of the high-latitude reconnection site, also known as the merging gap, sometimes visible as an auroral spot [*Milan et al.*, 2000]; the thin arrowed curves show the ionospheric convection excited by this reconnection. We show here the situation for $B_y > 0$, $|B_y| < B_z$, appropriate some time after the arc first formed. Plasma flows sunward across the merging gap and is then diverted east and west to form the two reverse convection cells. In the postnoon cell, plasma and flux is "stirred" as expected. In the prenoon cell, however, plasma is transferred from the dusk polar cap to the dawn polar cap, causing the former to contract and the latter to expand. Flow streamlines crossing the OCB, including the transpolar arc, are adiaroic ("not flowing across") indicating that the arc moves with the plasma flow, from dawn to dusk. In this scenario, in the absence of nightside reconnection, the overall polar cap remains of constant size.

[26] In Figure 7a, an indentation is shown in the northern lobe, representing open field lines which have been removed from the down-tail lobe by high-latitude reconnection occurring at the dayside magnetopause. This open flux is not destroyed but is carried to the east and west by the flow of the solar wind (for $|B_y| < B_z$) and laid on the magnetopause as two protuberances. Pressure exerted on the magnetopause by the surrounding solar wind causes the tail to revert to a near-circular cross section, which requires flows inside the lobe that redistribute the flux within and cause the transpolar arc to move. If the picture was to be redrawn for the case of $|B_y| > B_z$, then the removal of flux would be displaced to dawn (dusk) for $B_y > 0$ nT ($B_y < 0$ nT), and the corresponding readdition of flux would occur at dusk (dawn). The resulting flows in the Northern Hemi-

sphere ionosphere would take the form of single lobe cell with clockwise (anticlockwise) convection, as predicted by, e.g., *Reiff and Burch* [1985] and *Cowley and Lockwood* [1992]. In Figures 9a and 9b we contrast the ionospheric flow patterns expected for $|B_y| < B_z$ and $|B_y| > B_z$, in these cases for $B_y > 0$. The redistribution of flux in the polar cap and in the magnetotail implied by these sketches suggests that in the latter case a transpolar arc could move all the way from dusk to dawn, or vice versa depending on the orientation of B_y, whereas in the former case, arc motion will be toward the noon-midnight meridian of the polar cap but no further, irrespective of B_y and the initial location of the arc.

[27] The rate at which flux is transferred from the dusk to dawn polar caps can then be determined from the flux measurements of Figure 4. This should correspond to the lobe reconnection rate associated with the dawn lobe cell, which we will refer to as Φ_B, though we should not forget that there will be a reconnection rate associated with the dusk cell also, but this does not contribute to the motion of the transpolar arc. The rate of expansion of the dawn sector polar cap will be equal to Φ_B. The rate of contraction of the dusk sector polar cap has two contributions: Φ_B, as flux is siphoned to the dawn cell, and the contraction caused by the nightside reconnection Φ_C associated with the TRINNI, which occurs solely from the dusk cell (see, e.g., Figures 5a–5c). Thus we are able to write

$$\frac{dF_{\text{dawn}}}{dt} = \Phi_B$$
$$\frac{dF_{\text{dusk}}}{dt} = -\Phi_B - \Phi_C. \tag{4}$$

We can also attempt to determine Φ_B from the IMF observations in the same manner as Φ_A in equation (2). *Milan* [2004b] suggested that

$$\Phi_B = V_x B_N L_B, \tag{5}$$

where B_N is the northward component of the IMF (compare to equation (3)) and L_B is the effective length of the high-latitude reconnection site. We find that $L_B = 0.5\ R_E$ is a good fit for the observations; Figure 4b shows Φ_B calculated using this value. Equation (4) can then be used to find F_{dawn} and F_{dusk} (set initially to 0 and F_{PC}, respectively), which are overlaid as thin solid curves in Figure 4a.

[28] The expected flow pattern associated with combined lobe and nightside reconnection is shown in Figure 8b, appropriate for $B_y < 0$, $|B_y| < B_z$, the IMF orientation during the TRINNI. The former stirs flux within the polar cap; the latter causes an overall contraction of the whole polar cap, though in this case the merging gap is confined to the dusk side of the transpolar arc. The flows across the nightside merging gap are diverted toward dusk, as the observations of *Grocott et al.* [2003, 2004] suggest, unlike substorm-associated reconnection, in which flows would be diverted to both dusk and dawn, forming the nightside portion of the twin-cell convection pattern. The sketched flows are in close agreement with the observations in Figures 5b–5d.

[29] The values of Φ_B found in Figure 4b can be compared with estimates of the associated convection voltage from the SuperDARN observations. From the potential solutions indicated in Figure 5 we determine the potential difference between the center of the dawn lobe cell (which appears to be located near the sunward end of the transpolar arc), shown as a diamond in Figures 8a and 8b, and the point at which flow is deflected either dawnward or duskward as it passes sunward across the lobe merging gap, shown by a circle. Throughout the period 0730–1200 UT this varies between 10 and 20 kV, in close agreement with the values of Φ_B inferred from the changes in size of the dawn and dusk polar caps and calculated from equation (5) for $L_B = 0.5$ R_E, as shown in Figure 4b. We consider this to be strong evidence for the validity of our model of transpolar arc motion. We should remember that Φ_B and L_B are appropriate solely for the dawn reverse cell. The total lobe reconnection rate, and the potential difference between the centers of the dawn and dusk reverse cells (diamonds and squares in Figure 8), will be approximately double these estimates, giving an overall magnetopause merging line length of ~ 1 R_E.

[30] By way of comparison, *Chisham et al.* [2004] employed SuperDARN radar observations to measure a lobe reconnection rate of ~ 15 kV, for a period of IMF $B_z \approx 5$ nT and a solar wind speed of 350 km s^{-1}. Again, this is consistent with an effective lobe merging line length of ~ 1 R_E. We contrast these estimates of the effective length of the merging line (the length along which integration of the solar wind motional electric field equals the rate of flux transfer observed in the ionosphere) with an actual high-latitude merging line length of ~ 4 R_E deduced by *Phan et al.* [2003] for an interval on 18 March 2002. An effective merging line length is not known for the interval of Phan et al., as no simultaneous measurement of lobe reconnection rate was made, but the discrepancy between actual and effective lengths possibly points to a high-latitude reconnection efficiency of $\sim 25\%$, similar to that deduced for low-latitude reconnection, as discussed in section 3.1.

[31] Before moving on, we should emphasize that the lobe reconnection rate will probably differ between northern and southern lobes. Lobe reconnection might be expected to occur preferentially in the northern (southern) lobe for IMF $B_x < 0$ nT ($B_x > 0$ nT), as suggested by *Reiff and Burch* [1985]. During most of the present interval, $B_x < 0$ nT, and lobe reconnection is indeed active in the Northern Hemisphere. We expect that lobe reconnection is inactive, or active at a reduced rate, in the southern lobe, though our observations do not allow this to be investigated. In other words, L_B, the effective length of the lobe reconnection site, can be different for the two lobes, and may be a function of B_x, though more observations will be needed to confirm this. However, this discussion does suggest that the motion of transpolar arcs will be different in the northern and southern lobes, dependent on B_x, and that their auroral configuration in the northern and southern polar caps may not appear to remain conjugate (e.g., nonconjugacy has been observed by *Østgaard et al.* [2003]), though we expect that the transpolar arcs will still map magnetically to each other. This is indicated in Figure 7a, which shows lobe reconnection in the Northern Hemisphere, and the corresponding motion of the northern transpolar arc, but with no reconnection or arc motion in the Southern Hemisphere.

3.4. Fate of the Transpolar Arc

[32] Finally, we turn our attention to the interval after 1145 UT when the IMF turns southward. The expected flow pattern and response of the polar cap flux is shown in Figure 8c. The low-latitude merging gap now extends along the dayside OCB, with flow crossing from the closed flux region to the open as field lines are opened, and the polar cap as a whole expands with time. We expect at this time that the open/closed flux regions associated with the preexisting polar cap and transpolar arc are shunted to the nightside by the addition of new open flux. The boundary between new and old open flux is indicated in Figure 8c by a thin dashed curve. The corresponding situation in the tail is shown in Figure 7b; here equal amounts of flux have been added to both northern and southern lobes, as required for low-latitude reconnection. The flows which redistribute the flux to give the tail a circular cross section, and which correspond to the antisunward flows in the polar cap, are also indicated. The auroral observations show that at this time the sunward end of the transpolar arc becomes bent toward the noon-midnight meridian by the impinging new open flux (see Figure 8c), and it is this that is observed as the faint auroral structure crossing the polar cap from the dayside to the nightside, indicated by the arrow in Figure 3a, effectively marking the boundary between preexisting and new open flux. The motion of this boundary in the keogram of Figure 3a graphically demonstrates the open flux throughput of the magnetosphere, as it is created on the dayside and subsequently destroyed on the nightside following the substorm onset at 1245 UT. The nightside reconnection rate during this substorm interval is ~ 100 kV, which we contrast with 35 kV observed during the TRINNI earlier in the interval.

4. Summary and Conclusions

[33] We summarize the conclusions of this study as follows:

[34] 1. During a burst of tail reconnection, in the absence of normal substorm indicators, occurring under northward IMF conditions (which we name a TRINNI), a transpolar arc forms. Such reconnection bursts have previously been observed by *Grocott et al.* [2003, 2004], who surmised that the penetration of IMF B_y into the magnetotail results in closed field lines which are distorted out of meridian planes following tail reconnection. We speculate that this could lead to a buildup of closed flux that is unable to convect normally in the return flow regions due to competition between the conjugate hemispheres, resulting in tongues of closed flux protruding from the plasma sheet.

[35] 2. Subsequent motion of the transpolar arc is controlled by the rate of lobe reconnection and the associated transport of open flux from one side of the arc to the other. To a first approximation, if IMF $B_y > 0$ nT, then open flux is siphoned from dusk to dawn (the lobe convection cell rotates clockwise) and arc motion will be from dawn to dusk, and vice versa for $B_y < 0$ nT. However, the exact details of the motion will depend on the location of the arc relative to the lobe merging gap. If $|B_y| > B_z$, then the

merging gap will be displaced far toward dawn or dusk, a single lobe convection cell exists, and open flux can be transported easily from one side of an arc to the other. Alternatively, if $|B_y| < B_z$, then the merging gap will be placed near noon, a twin-cell lobe pattern results, and it might be expected that transpolar arcs will move toward the noon-midnight meridian, irrespective of whether they are located in the dawn or dusk sectors, and irrespective of the orientation of B_y. In addition, transpolar arc motion in the two hemispheres might not appear conjugate (though magnetic mapping between the two hemispheres will be) if the rates of lobe reconnection differ in the north and south.

[36] 3. Tail reconnection in the presence of a transpolar arc appears confined to dawnward or duskward of the arc. This is true of reconnection bursts during substorm and nonsubstorm intervals.

[37] 4. The motion of the transpolar arc allows the lobe reconnection rate to be estimated. The total lobe reconnection rate, $\sim$20–40 kV, is consistent with the solar wind motional electric field integrated along a merging gap with an effective length of $\sim$1 R_E, close to the suggestion of *Milan* [2004a] and consistent with the measurement of *Chisham et al.* [2004]. In the present case, with $|B_y| < B_z$, this reconnection voltage is roughly equally partitioned between twin reverse convection cells. For $|B_y| > B_z$, a single lobe cell is expected, driven by the full reconnection voltage. The effective merging gap length is probably a function of IMF B_x, and will usually differ between hemispheres. The observation by *Phan et al.* [2003] of a high-latitude merging line of length $\sim$4 R_E might imply that reconnection efficiency at high latitudes is close to 25%, similar to that found at low latitudes (see point 5 below).

[38] 5. In contrast, the effective length of the low-latitude merging gap is $\sim$5 R_E, $\sim$20–25% of the width of the dayside magnetosphere, as previously reported by, e.g., *Holzer and Slavin* [1979], *Reiff et al.* [1981], *Milan et al.* [2004], and *Milan* [2004a, 2004b].

[39] 6. The tail reconnection rate is estimated as $\sim$35 kV during nonsubstorm bursts (TRINNIs), and as $\sim$100 kV during substorms, again similar to previous estimates [e.g., *Milan et al.*, 2003, 2004; *Grocott et al.*, 2003, 2004; *Milan*, 2004a, 2004b].

[40] Further study is needed to confirm a link between TRINNI occurrence and transpolar arc formation. However, both are expected to occur under northward IMF conditions, and the proposed formation mechanism predicts that arcs should form at dawn for $B_y < 0$ and dusk for $B_y > 0$ (in the Northern Hemisphere), consistent with previous reports [e.g., *Kullen et al.*, 2002]. Arc motion is subsequently controlled by the rate of lobe reconnection, also a phenomenon associated with northward IMF and controlled by the sense of B_y. The arc is not expected to disappear immediately at the next southward turning of the IMF, but the redistribution of flux caused by subsolar reconnection and (especially) substorm processes will cause a gradual reassimilation of the closed flux of the arc with the closed flux of the plasma sheet. The present work has presented a framework within which to understand arc formation and motion, with specific predictions that can be tested by subsequent studies.

References

Chisham, G., M. P. Freeman, I. J. Coleman, M. Pinnock, M. R. Hairston, M. Lester, and G. Sofko (2004), Measuring the dayside reconnection rate during an interval of due northward interplanetary magnetic field, *Ann. Geophys.*, 22, 4243–4258.

Cowley, S. W. H. (1981), Magnetospheric and ionospheric flow and the interplanetary magnetic field, in *The Physical Basis of the Ionosphere in the Solar-Terrestrial System*, AGARD Conf. Proc., CP-295, 4, 1–14.

Cowley, S. W. H., and M. Lockwood (1992), Excitation and decay of solar wind-driven flows in the magnetosphere-ionosphere system, *Ann. Geophys.*, 10, 103–115.

Frank, L. A., J. D. Craven, J. L. Burch, and J. D. Winningham (1982), Polar views of the Earth's aurora with Dynamics Explorer, *Geophys. Res. Lett.*, 9, 1001–1004.

Frank, L. A., et al. (1986), The theta aurora, *J. Geophys. Res.*, 91, 3177–3224.

Greenwald, R. A., et al. (1995), DARN/SuperDARN: A global view of the dynamics of high-latitude convection, *Space Sci. Rev.*, 71, 761–796.

Grocott, A., S. W. H. Cowley, and J. B. Sigwarth (2003), Ionospheric flow during extended intervals of northward but B_y-dominated IMF, *Ann. Geophys.*, 21, 509–538.

Grocott, A., S. V. Badman, S. W. H. Cowley, T. K. Yeoman, and P. J. Cripps (2004), The influence of IMF B_y on the nature of the nightside high-latitude ionospheric flow during intervals of positive IMF B_z, *Ann. Geophys.*, 22, 1755–1764.

Holzer, R. E., and J. A. Slavin (1979), A correlative study of magnetic flux transfer in the magnetosphere, *J. Geophys. Res.*, 84, 2573–2578.

Huang, C.-S., G. J. Sofko, A. V. Koustov, D. A. Andre, J. M. Ruohoniemi, R. A. Greenwald, and M. R. Hairston (2000), Evolution of ionospheric multicell convection during northward interplanetary magnetic field with $|B_z/B_y| > 1$, *J. Geophys. Res.*, 105, 27,095–27,107.

Huang, C. Y., L. A. Frank, W. K. Petersen, D. J. Williams, W. Lennartsson, D. G. Mitchell, R. C. Elphic, and C. T. Russell (1987), Filamentary structures in the magnetotail lobes, *J. Geophys. Res.*, 92, 2349–2363.

Kullen, A., M. Brittnacher, J. A. Cumnock, and L. G. Blomberg (2002), Solar wind dependence of the occurrence and motion of polar auroral arcs: A statistical study, *J. Geophys. Res.*, 107(A11), 1362, doi:10.1029/2002JA009245.

McComas, D. J., S. J. Bame, P. Barker, W. C. Feldman, and J. L. Philips (1998), Solar wind electron proton alpha monitor (SWEPAM) for the Advanced Composition Explorer, *Space Sci. Rev.*, 86, 563.

Mende, S. B., et al. (2000a), Far ultraviolet imaging from the IMAGE spacecraft. 1. System design, *Space Sci. Rev.*, 91, 243–270.

Mende, S. B., et al. (2000b), Far ultraviolet imaging from the IMAGE spacecraft. 2. Wideband FUV imaging, *Space Sci. Rev.*, 91, 271–285.

Milan, S. E. (2004a), A simple model of the flux content of the distant magnetotail, *J. Geophys. Res.*, 109, A07210, doi:10.1029/2004JA010397.

Milan, S. E. (2004b), Dayside and nightside contributions to the cross polar cap potential: Placing an upper limit on a viscous-like interaction, *Ann. Geophys.*, 22, 3771–3777.

Milan, S. E., M. Lester, S. W. H. Cowley, and M. Brittnacher (2000), Dayside convection and auroral morphology during an interval of northward interplanetary magnetic field, *Ann. Geophys.*, 18, 436–444.

Milan, S. E., M. Lester, S. W. H. Cowley, K. Oksavik, M. Brittnacher, R. A. Greenwald, G. Sofko, and J.-P. Villain (2003), Variations in polar cap area during two substorm cycles, *Ann. Geophys.*, 21, 1121–1140.

Milan, S. E., S. W. H. Cowley, M. Lester, D. M. Wright, J. A. Slavin, M. Fillingim, C. W. Carlson, and H. J. Singer (2004), Response of the magnetotail to changes in the open flux content of the magnetosphere, *J. Geophys. Res.*, 109, A04220, doi:10.1029/2003JA010350.

Mishin, V. M., et al. (1997), A study of the CDAW 9C substorm of May 3, 1986, using magnetogram inversion technique 2, and a substorm scenario with two active phases, *J. Geophys. Res.*, 102, 19,845–19,859.

Østgaard, N., S. B. Mende, H. U. Frey, L. A. Frank, and J. B. Sigwarth (2003), Observations of non-conjugate theta aurora, *Geophys. Res. Lett.*, 30(21), 2125, doi:10.1029/2003GL017914.

Phan, T., et al. (2003), Simultaneous Cluster and IMAGE observations of cusp reconnection and auroral proton spot for northward IMF, *Geophys. Res. Lett.*, *30*(10), 1509, doi:10.1029/2003GL016885.

Rairden, R. L., and S. B. Mende (1989), Properties of 6300-Å auroral emission at South Pole, *J. Geophys. Res.*, *94*, 1402–1416.

Reiff, P. H., and J. L. Burch (1985), IMF B_y-dependent plasma flow and Birkeland currents in the dayside magnetosphere: 2. A global model for northward and southward IMF, *J. Geophys. Res.*, *90*, 1595–1609.

Reiff, P. H., R. W. Spiro, and T. W. Hill (1981), Dependence of polar cap potential drop on interplanetary parameters, *J. Geophys. Res.*, *86*, 7639–7648.

Ruohoniemi, J. M., and K. B. Baker (1998), Large-scale imaging of high-latitude convection with Super Dual Auroral Radar Network HF radar observations, *J. Geophys. Res.*, *103*, 20,797–20,811.

Russell, C. T. (1972), The configuration of the magnetosphere, in *Critical Problems of Magnetospheric Physics*, edited by E. R. Dyer, p. 1, Inter-Union Comm. on Sol. Terr. Phys., Natl. Acad. of Sci., Washington, D. C.

Samson, J. C., D. D. Wallis, T. J. Hughes, F. Creutzberg, J. M. Ruohoniemi, and R. S. Greenwald (1992), Substorm intensifications and field line resonances in the nightside magnetosphere, *J. Geophys. Res.*, *97*, 8495–8518.

Senior, C., J.-C. Cerisier, F. Rich, M. Lester, and G. K. Parks (2002), Strong sunward propagating flow bursts in the night sector during quiet solar wind conditions, SuperDARN and satellite observations, *Ann. Geophys.*, *20*, 771–779.

Siscoe, G. L., and T. S. Huang (1985), Polar cap inflation and deflation, *J. Geophys. Res.*, *90*, 543–547.

Smith, C. W., J. L'Heureux, N. F. Ness, M. H. Acuña, L. F. Burlaga, and J. Scheifele (1998), The ACE Magnetic Field Experiment, *Space Sci. Rev.*, *86*, 613–632.

Taylor, J. R., T. K. Yeoman, M. Lester, B. A. Emery, and D. J. Knipp (1996), Variations in the polar cap area during intervals of substorm activity on 20–21 March 1990 deduced from AMIE convection maps, *Ann. Geophys.*, *14*, 879–887.

Valladares, C. E., H. C. Carlson, and K. Fukui (1994), Interplanetary magnetic field dependency of stable Sun-aligned polar cap arcs, *J. Geophys. Res.*, *99*, 6247–6272.

Zhu, L., R. W. Schunk, and J. J. Sojka (1997), Polar cap arcs: A review, *J. Atmos. Sol. Terr. Phys.*, *59*, 1087–1126.

————————

A. Grocott, B. Hubert, and S. E. Milan, Department of Physics and Astronomy, University of Leicester, University Road, Leicester LE1 7RH, UK. (steve.milan@ion.le.ac.uk)